Effect of paint baking treatment on the properties of press hardened boron steels

Henri Järvinen[1]*, Mari Honkanen[1], Martti Järvenpää[2], and Pasi Peura[1]

[1]Laboratory of Materials Science, Tampere University of Technology

P.O. Box 589, FI-33101 Tampere, Finland

[2]SSAB Europe Oy, Harvialantie 420, FI-13300, Hämeenlinna, Finland

[1*)] henri.jarvinen@tut.fi

ABSTRACT

This study comprehends the effect of a typical paint baking process on the properties of press hardened boron steels. Bake hardening response of four 22MnB5 steels with different production histories and two other boron steels of 30MnB5 and 34MnB5 type were analyzed. In particular, the effect of steel carbon content and prior austenite grain size on the strength of the bake hardening treated steels was investigated. Press hardened steels showed a relatively strong bake hardening effect, 80–160 MPa, in terms of yield strength. In addition, a clear decrease in ultimate tensile strength, 30–150 MPa, was observed due to baking. The changes in tensile strength showed a dependency on the carbon content of the steel: higher carbon content led to a larger decrease in tensile strength in general. Smaller prior austenite grain size resulted in a higher increase in yield strength despite the micro-alloyed 34MnB5. Transmission electron microscopy analysis carried out for the 34MnB5 revealed niobium rich mixture carbides of (Nb, Ti)C, which have most likely influenced the different bake hardening response. The present results indicate that the bake hardening response of press hardened steels depends on both prior austenite grain size and carbon content, but is also affected by other alloying elements. The observed correlation between prior austenite grain size and bake hardening response can be used to optimize the production of the standard grades of 22MnB5 and 30MnB5. In addition, our study suggests that baking process improves the post-uniform elongation and ductile fracture behavior of 34MnB5, but do not significantly influence the ductile fracture mechanisms of 22MnB5 and 30MnB5 representing lower strength levels.

KEYWORDS: Press hardening; Bake hardening; Paint baking; Martensite; EBSD; Prior austenite grain size

1. INTRODUCTION

In recent years, the automotive industry has faced increasing demand to reduce CO_2 emissions and at the same time to improve safety performance of passenger cars (Åkerström, 2006). The increased use of press hardening steels (PHS) in the car body has proven to be an appropriate solution to meet these requirements. The components produced by using the direct press hardening process are first austenitized at around 900–950 °C for 3–10 minutes (Fan et al., 2009). After that, the blank is transferred rapidly to the press in which it is subsequently hot-press formed and quenched in a die. The martensitic phase transformation leads to the ultra-high tensile strength of around 1500 MPa (Fan et al., 2009). Nevertheless, the in-service properties of PHS are finalized in a subsequent paint baking process characteristic to the serial production of car body components (Fan et al., 2009). The thermal cycle of paint baking, 150–190 °C for 15–60 min, enhance a diffusion-controlled aging phenomena being responsible for the bake hardening (BH) effect (Kantereit, 2011). This effect needs to be considered as a part of steel and component design (8). In the case of PHS, the paint baking process can be considered as an additional low-temperature tempering (LTT) process usually simulated with a 20 min soak at 170 ˚C.

In general, bake hardening is a well-known strengthening mechanism, which is based on the phenomena of static strain aging (SSA) (Baker et al., 2002). It has been used in the automotive steels when reaching the maximum strength of formed components (Kantereit, 2011). In the case of low carbon ferritic steels, the attainable yield strength increase is attributed to the diffusion of solute carbon and nitrogen atoms, enhanced by elevated paint baking temperatures, and their interactions with priory introduced dislocations (Wilson and Russell, 1960a). SSA may influence the mechanical properties of steel via three distinct mechanisms occurring as a function of aging time and temperature. The first mechanism, strain induced ordering of solute atoms, was originally introduced by Snoek (1941). The understanding of the so-called Snoek effect was later extended by Wilson et al. (1959) who observed that the strain aging of low carbon steel is contributed to stress induced ordering of solute atoms. The second contributing mechanism was introduced by Cottrell and Bilby (1949) who notified that strain aging is involved with the dislocation pinning effect, which is generated by interactions between interstitial atoms and existing mobile dislocations. This phenomenon, known today as Cottrell atmosphere formation, was studied later on by Wilson and Russell (1960a). They observed that the Cottrell atmosphere formation led to the locking of mobile dislocations in a 4 % strained rimming steel. Concerning practical applications, the dislocation pinning effect leads to the increased yield strength, which is characteristic to the BH effect of low carbon steels (Baker et al., 2002). According to Wilson and

Russell (1960b), the third mechanism behind SSA is the formation of solute clusters finally resulting in the precipitation of fine transition carbides. Ever since, the theories discussed above have been elaborated and used in order to understand the BH behavior of various automotive steels.

Currently, it is known that the BH response of a given steel grade depends on a variety of adjustable characteristics (Baker et al., 2002). These are phases present, amount of solute carbon, grain size, and dislocation density. Thus, the BH behavior of ultra-low carbon ferritic steels, reviewed by (Baker et al., 2002), is significantly different from high-strength multiphase steels analyzed for example by Timoknina et al. (2008), and fully martensitic steels reported by Hagström and Ryde (2008). In particular, the precipitation stage has been difficult to confirm in low carbon ferritic steels (Baker et al., 2002), whereas the precipitation of fine transition carbides during the LTT processes (150–200 ˚C) of martensitic steels has been confirmed (Krauss, 1995). For instance, Sherman et al. (1983) investigated the static aging behavior of Fe-Ni-C martensites and observed that fine transition carbides, i.e., ε-carbides were formed in the first stage of tempering at temperatures above 100 ˚C. The scientists presented that the formation of coarser Fe_3C carbides occurs at higher aging temperatures and can compete with the ε-carbide formation. Timoknina et al. (2008) observed the formation of both fine and coarse Fe_3C carbides within the martensitic constituents (16) of ferritic-martensitic DP steels, after baking at 175 ˚C for 30 min. This behavior can be connected with a relatively high carbon content of martensite (16). At present, it is also clear that the high dislocation density and fine grain size of bainite and martensite (16) enhances a relatively strong BH effect even without any externally applied pre-strain, which is essentially required to cause the BH response of low carbon ferritic steels. For example, Das et al. (2012) investigated the BH behavior of TRIP (Transformation Induced Plasticity) steels and showed that the dislocations generated during the bainite transformation can induce a strong BH response. Hagström and Ryde (2008), in turn, reported about 10 % increase in yield strength for non-deformed martensitic steels.

According to the theoretical background discussed above, three principal mechanisms may have a role in the BH behavior of press hardened boron steels: dislocation locking caused by the formation of Cottrell atmospheres, precipitation of iron carbides, and softening of martensitic matrix. As noted by Krauss (1995), the last two are interdependent mechanisms, since the tetragonality of martensite lattice decreases as carbon atoms migrate from octahedral interstitial sites towards solute clusters – finally to form precipitates. Previous studies have shown that martensitic steels can exhibit a special SSA behavior due to high dislocation density and fine grain size. To clarify, Miller et al. (1983) observed that carbon atoms of Fe-Ni-C alloy segregated towards lath boundaries already during quenching. Wilde et al. (2000) confirmed that the Cottrell atmosphere formation occurred readily during quenching in high purity 0.10–0.18 C % steels, at cores of fresh transformation-induced dislocations located particularly in lath boundaries. The more recent study of Hutchinson et al. (2011) support the earlier observations by showing that the same phenomenon occurs in martensitic C-Mn steels with carbon contents of 0.1–0.5 %.

Assuming the earlier findings discussed above, there are two dominant mechanisms controlling the BH effect of PHS: the precipitation of fine iron carbides and the softening of martensitic matrix. Choi et al. (2015) focused on the BH behavior of 22MnB5 by using the internal friction method. The scientists suggested that the kinetics of Cottrell atmosphere formation and precipitation of transition carbides is much faster in press hardened 22MnB5 steel than in low carbon ferritic steels. This was explained by fine grain size and high dislocation density of martensite. In addition, their results show that there clearly exists an internal friction peak already in a die quenched condition caused by the interactions between dislocations and carbon interstitials. (1) The study of Sulistiyo et al. (2016) support earlier observations and show that carbon atoms of 0.31 % C PHS diffuse to the dislocation cores already during die quenching and enable simultaneous auto-tempering of martensite, which is characteristic to the direct press hardening process. These findings suggest that both grain size and carbon content of martensitic steels have a significant effect on the BH kinetics, and thus they have a role in determining the BH response of PHS.

Understanding of the mechanisms behind SSA are essential in order to control the BH behavior of PHS. Traditionally, the BH effect of ferritic low carbon steels has been controlled by using an adequate content of solute carbon (Baker et al., 2002) However, Hanai et al. (1984) were able to control the BH response of aluminium-killed low-carbon steel by optimizing both the amount of interstitials and the ferrite grain size of the steel. They reported that smaller grain size increased the BH effect in terms of yield strength, especially when the amount of interstitials in solid solution was at least 10 ppm. Kinoshita and Nishimoto (1990) extended the understanding of the role of ferrite grain size by suggesting that the BH response of cold-rolled low carbon steels might depend on both solute carbon content and the amount of carbon segregated to the grain boundaries. Later on De et al. (2004) observed that the grain size variation has effect on the carbon distribution between grain interior and grain boundaries. They concluded that the BH effect of ultra-low carbon steel increases with decreasing grain size especially when critical values of grain size and pre-strain, i.e., dislocation density and distribution are met. According to Baker et al. (2002) the grain size has a relatively complex role in bake hardening since it does not only influence the diffusion distance between carbon and dislocations, but also affects the dislocation density and distribution of the steel. Unfortunately, the number of studies addressing the grain size effects in the bake hardening behavior of martensitic steels seems to be very small. Hagström and Ryde (2008) have reported the enhanced bake hardenability of martensitic steels with respect to the finer grain size. However, previous studies have not quantitatively addressed the relationships between the grain size and the BH effect of PHS until further notice. The bake hardening response has not been either connected with the parameters of the direct press hardening process.

Eventually, it seems that there is not much information available either on the significance of processing parameters or chemical composition to the BH effect of PHS. The purpose of our study is to analyze the effect of prior austenite grain size (PAGS) and carbon content on the BH response of a number of PHS. Thus, the results of this study aim to provide a link between the austenitizing parameters of the direct press hardening process and BH effect. In the present study (17), typical process parameters to the direct press hardening and paint baking are studied. Finally, the bake hardening effect and tensile behavior of the investigated steels are discussed in detail.

2. MATERIALS AND EXPERIMENTAL PROCEDURES

2.1 AS-RECEIVED MATERIAL PROPERTIES

The test materials of this study comprised (9) six commercially produced press hardenable steels. The samples were received as 1.5–2.3 mm thick steel sheets. Initial properties and chemical compositions of the sample materials are given in Table 1. The as-received 22MnB5 grades had the same nominal chemical compositions. However, small variation in carbon contents (0.23–0.25 %), for example, existed. In this paper, the 22MnB5 grades are named using the same prefix of 1. Accordingly, steel 1-FH (full hard) was received as cold-rolled (CR), while materials 1-CA_1 and 1-CA_2 were received as cold-rolled and continuously annealed (CA). Steel 1-BA (batch annealed) was received as sub-critically annealed, i.e. the annealing had been carried out in a batch furnace. In addition to the 22MnB5 grades, a boron-alloyed steel grade of 30MnB5 type was received as hot-rolled (HR) and direct-quenched (DQ). This steel is called 2-DQ in this paper. A steel grade of 34MnB5 type was supplied as cold-rolled and continuously annealed. This grade is referred to as 3-CA_3 (continuously $annealed_3$) in this paper.

Table 1. (18) As-received conditions and chemical compositions for the investigated steels. In the "Phases present" column, F refers to ferrite, P to pearlite, C to cementite, and M to martensite. A_{c1} and A_{c3} temperatures were calculated using JMatPro® software (Saunders et al., 2003).

22MnB5 grades											
Steel	**Production history**	**Phases present**	**Thickness (mm)**	**C %**	**Si %**	**Mn %**	**Cr %**	**B %**	**Ti %**	**A_{c1}(°C)**	**A_{c3}(°C)**
1-FH	CR	F+P+C	1.7	0.24	0.25	1.24	0.20	0.0027	0.034	713	804
1-CA_1	CR+CA_1	F+P+C	1.5	0.23	0.24	1.23	0.21	0.0027	0.029	714	805
1-CA_2	CR+CA_2	F+P+C	1.5	0.23	0.26	1.24	0.21	0.0031	0.040	715	810
1-BA	CR+BA	F+C	1.5	0.25	0.26	1.20	0.29	0.0022	0.039	719	806
Reference grade of 30MnB5											
Steel	**Production history**	**Phases present**	**Thickness (mm)**	**C %**	**Si %**	**Mn %**	**Cr %**	**Ti+V+Nb %**		**A_{c1}(°C)**	**A_{c3}(°C)**
2-DQ	HR+DQ	M	2.3	0.29	0.21	1.20	0.66	0.035		728	791
Reference grade of 34MnB5											
Steel	**Production history**	**Phases present**	**Thickness (mm)**	**C %**		**Mn %**		**Ti+V+Nb %**		**A_{c1}(°C)**	**A_{c3}(°C)**
3-CA_3	CR+CA_3	F+P+C	1.5	0.35		1.32		0.060		717	782

Microstructures of the investigated steels in as-received condition are presented in Fig. 1. The as-received samples were mechanically grinded, polished, and etched with 4 % Nital. (10) The microstructures of the 22MnB5 steels (Fig. 1a–1d) consists

of ferrite and pearlite/cementite in various morphologies. The direct-quenched steel 2-DQ shows a typical microstructure of lath martensite (Fig. 1e). The 3-CA_3 steel consists of ferrite, pearlite and cementite (Fig. 1f).

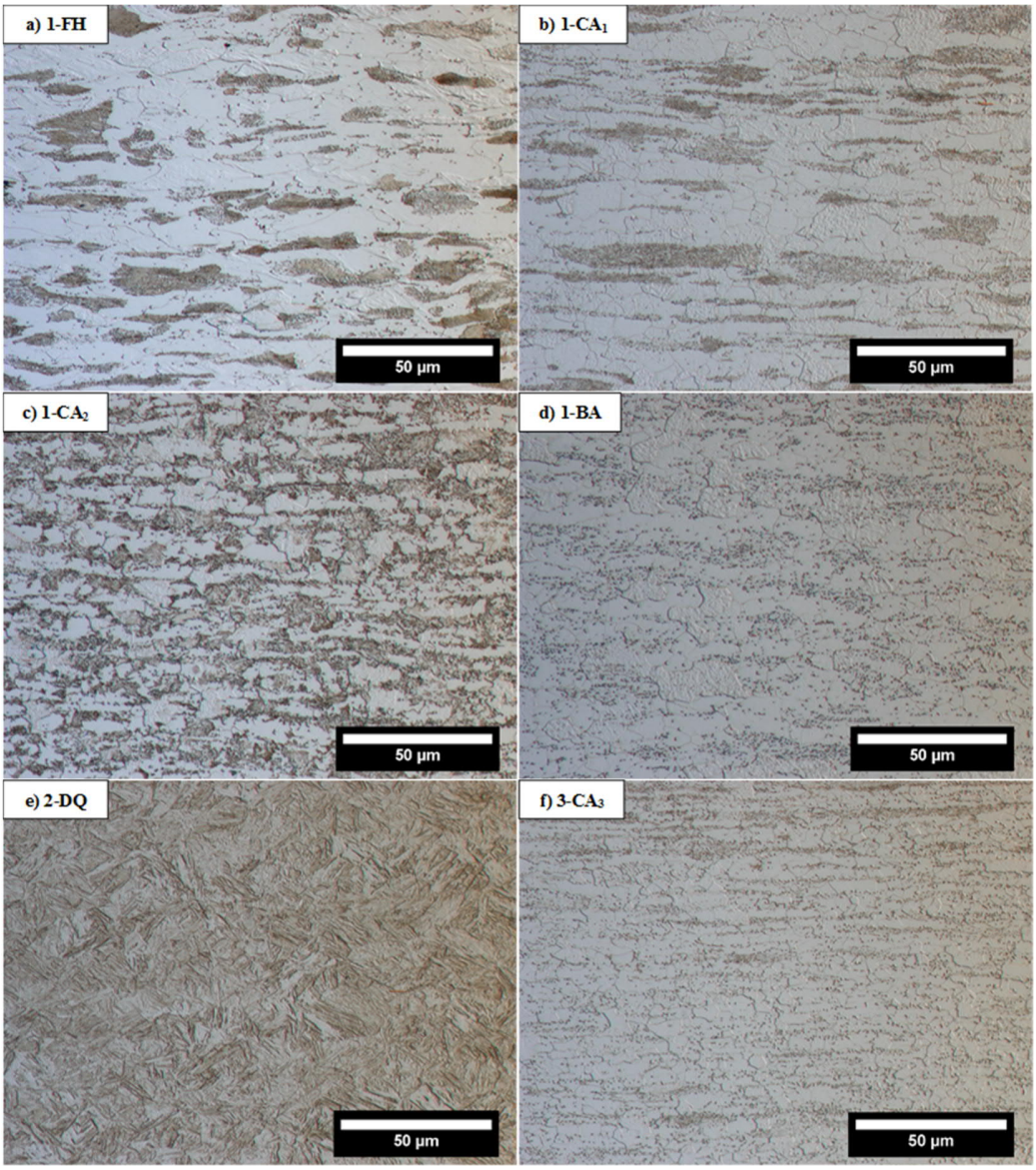

Fig. 1. (10) Optical micrographs of the as-received sample materials transverse to the rolling direction.

2.2 PRESS HARDENING EXPERIMENTS AND BAKE HARDENING HEAT TREATMENTS

The test materials of this study were subjected to the direct press hardening process and typical paint baking treatment. Press hardening experiments were first carried by using a custom-built press hardening equipment. Two different austenitization cycles, i.e., soaking times of 180 s and 450 s at 900 °C, were examined. Experiments were conducted for steel sheet samples

in two different sizes, namely 110 x 100 mm and 55 x 100 mm. The 110 x 100 mm sized samples were heat-treated in a furnace at 900 °C for 450 s and the 55 x 100 mm sized coupons at 900 °C for 180 s. The measured temperature of the sheet after the shorter austenitization time of 180 s was 895 ˚C, whereas in the case of longer austenitization time of 450 s, the target temperature of 900 ˚C was reached. (7) After the austenitizing, the sample was automatically transferred to the die and subsequently quenched between water-cooled steel blocks. A flat-die and a pressing force of 30 kN was used in die quenching step. The automated transferring and triggering of the die-quenching step enabled excellent repeatability of the experiments. (13) The equipment and experimental procedure of die quenching has been described more in detail in an earlier study (Järvinen et al., 2016).

A graph presented in Fig. 2a shows example cooling curves and synchronized compression force data for various steel sheet thicknesses of 1.5, 1.7 and 2.3 mm. As can be seen, thickness variation caused small variation in cooling rates particularly after reaching M_s temperature. There, the exothermic nature of the martensitic transformation naturally slows down the cooling rate. This phenomenon is emphasized by higher sheet thicknesses and can be thought to promote the auto-tempering of martensite. However, all the measured cooling rates exceeded the minimum average value of 50 °C/s between 900 ˚C and M_s, (Fig. 2a). Therefore, the attainment of fully martensitic microstructures were expected. The influence of different sample thicknesses is estimated to be relatively insignificant from the final properties point of view. For example, Bardelcik et al. (2010) have reported that the mechanical properties of 22MnB5 are insensitive to the cooling rate in the range of 45–250 °C/s.

The other set of the press hardened samples were subsequently baked following the specifications of EN 10325-2006. It is worth noting that the press hardened samples were not subjected to any pre-straining in order to meet the industrial conditions of hot-press formed components. Thus, the used BH procedure consisted only of a simple heat treatment, namely 170 °C for 20 min, after which the samples were allowed to cool in the air to the room temperature. The mechanical properties after bake hardening were finally tensile tested in that condition and compared with the ones measured for die quenched samples. The heat-treatment cycles of press hardened (PH) and bake hardened (PH+BH) samples are presented schematically in Fig 2b.

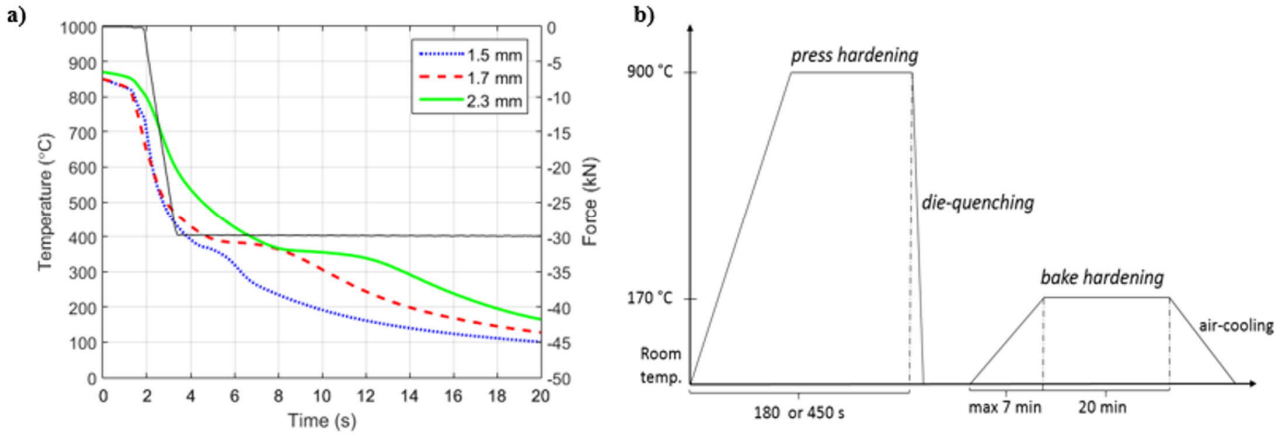

Fig. 2. a) (3) Example cooling curves and simultaneous pressing force evolution during die quenching for the sheet thicknesses of 1.5, 1.7 and 2.3 mm. b) Schematic presentation of the thermal cycle of press hardened (PH) and subsequently bake hardened samples (PH+BH).

2.3 MICROSTRUCTURAL ANALYSIS

Samples in both PH and PH+BH conditions were sectioned for the microstructural analysis carried out with an optical microscope Nikon Eclipse MA 100 and a scanning electron microscope (SEM) Zeiss Ultra Plus. The SEM was fitted with an HKL Premium-F Channel EBSD system equipped with a Nordlys F400 detector. The SEM was used to characterize microstructures and fracture surfaces. In addition, it was used electron backscatter diffraction (EBSD) analysis. The samples for both optical observations and SEM imaging were ground using abrasive SiC papers, final polished using diamond suspensions, and etched with Nital 4% solution.

The PH samples used in EBSD measurements were sectioned and final polished using colloidal silica suspension. Step sizes of 0.1–0.2 µm and acceleration voltages of 15 and 20 kV were used in the EBSD analysis carried out for the cross-sectional areas of 175 x 125 µm. The analyzed areas were located approximately in one-third of the thickness of the sheet. The EBSD analysis were carried out to both transverse and longitudinal directions in relation to the rolling direction of the as-received materials. The gathered EBSD-data of predominantly martensitic microstructures was used to reconstruct prior austenite grain boundary maps by using an algorithm script introduced by Nyyssönen et al. (2016). The reconstruction followed the procedure presented earlier (Järvinen et al., 2016). Mean linear intercepts (µm) were measured from the reconstructed grain boundary maps and used to represent prior austenite grain sizes (PAGS). Each grain size determination consisted of measuring 20 intercepts and the lines were drawn parallel to the vertical direction of prior austenite grain boundary maps. (11)

A transmission electron microscope (TEM) Jeol JEM-2010 equipped with an energy dispersive spectrometer (EDS, Noran Vantage Si(Li) detector, Thermo Scientific) was used to analyze the carbide structures of the selected samples in both PH and PH+BH conditions. TEM analysis was carried out after the mechanical testing had reveled somewhat different BH response between the investigated steels. (6) TEM samples were prepared using an extraction replica technique: the sample was polished by traditional metallographic method followed by etching (Nital 4% solution) to remove the matrix such that the carbides stand proud of the sample surface. Then, a carbon film was evaporated on the sample surface and scored into ~1 mm^2. After this, etching was continued to dissolve the matrix and the squares of the carbon film carrying the carbides with them were floated to the distilled water and collected on copper TEM grids. The compositions and structure of the precipitates were determined using EDS point measurements and selected area electron diffraction (SAED). An acceleration voltage of 200 kV was used in each case.

2.4 MECHANICAL TESTING

Microhardnesses (HV 0.5 kg) after press hardening were measured using a hardness tester Matsuzawa MMT-X7. Engineering stress-strain curves of both PH and PH+BH samples were measured using a quasistatic testing at the strain-rate of 5×10^{-4} s^{-1}. Tensile testing at room temperature was performed using a servo hydraulic materials testing machine Instron 8800. Load was measured using a 50 kN Instron load cell. A 6 mm gauge length extensometer was used to measure the elongation of the specimen gauge length.

Tensile test specimens with a gauge length of 8.0 mm and width of 2.0 mm were cut out of the PH samples using a water jet. The used sample geometry allows obtaining uniaxial constitutive data up to necking. Therefore, total elongation values expressed in the present study (17) are used only to evaluate material behavior in general and for comparison between the materials used here. Three tensile specimens in a PH condition were prepared from each of the larger die quenched sample sheets (110 x 100 mm) and three tensile tests were carried out per each test material austenitized for 450 s at 900 °C. Two tensile specimens were prepared from the smaller die quenched sample sheets (55 x 100 mm), respectively, and two repetition tests were carried out for each test material austenitized for 180 s at 900 °C. The same number of tensile test specimens were subjected to bake hardening heat treatments and following tensile testing in a PH+BH condition, respectively.

3. RESULTS

3.1 MICROSTRUCTURES

Based on the microstructural observations, fully martensitic microstructures were attained on the die quenched sample materials of 1-FH, 1-CA_1, 1-CA_2, 2-DQ, and 3-CA_3 austenitized for 180 s at 900 °C. The microstructure of 1-BA was not fully martensitic after the die quenching, i.e., in the PH condition. This result indicated on the incomplete austenitization process due to a short austenitization time of 180 s. To clarify this finding, ferrite islands (F) and undissolved cementite particles (C) were present (Fig 3a). The same finding has been discussed in an earlier study (Järvinen et al., 2016). In the case of longer austenitizing cycle, 450 s/900 °C, all the press hardened steels showed primarily martensitic microstructures. In fact, microstructures observed after the die quenching represented a mixture of martensite and auto-tempered martensite (Fig. 3b) as described in an earlier study of Järvinen et al. (2016) as well as in the study carried out by Matsuda et al. (2013). Example SEM micrographs revealing the microstructures of both PH and PH+BH samples of the steel 1-FH, austenitized for 450 s at 900 °C, are presented in Fig. 3c and 3d. A comparison between the microstructures of the PH (Fig. 3c) and the PH+BH (Fig 3d) condition reveals no clearly identifiable differences in micro-constituents: both samples consist of auto-tempered and fresh martensite. The precipitation of fine iron carbides within martensite laths, corresponding to the ones observed by Choi et al. (2015), are also identifiable in both conditions. However, the carbides within fresh martensite laths designated as (1) are better recognizable and in the PH+BH condition, whereas the carbides located in the auto-tempered areas designated as (2) are filled with fine iron carbides of the same appearance in both conditions.

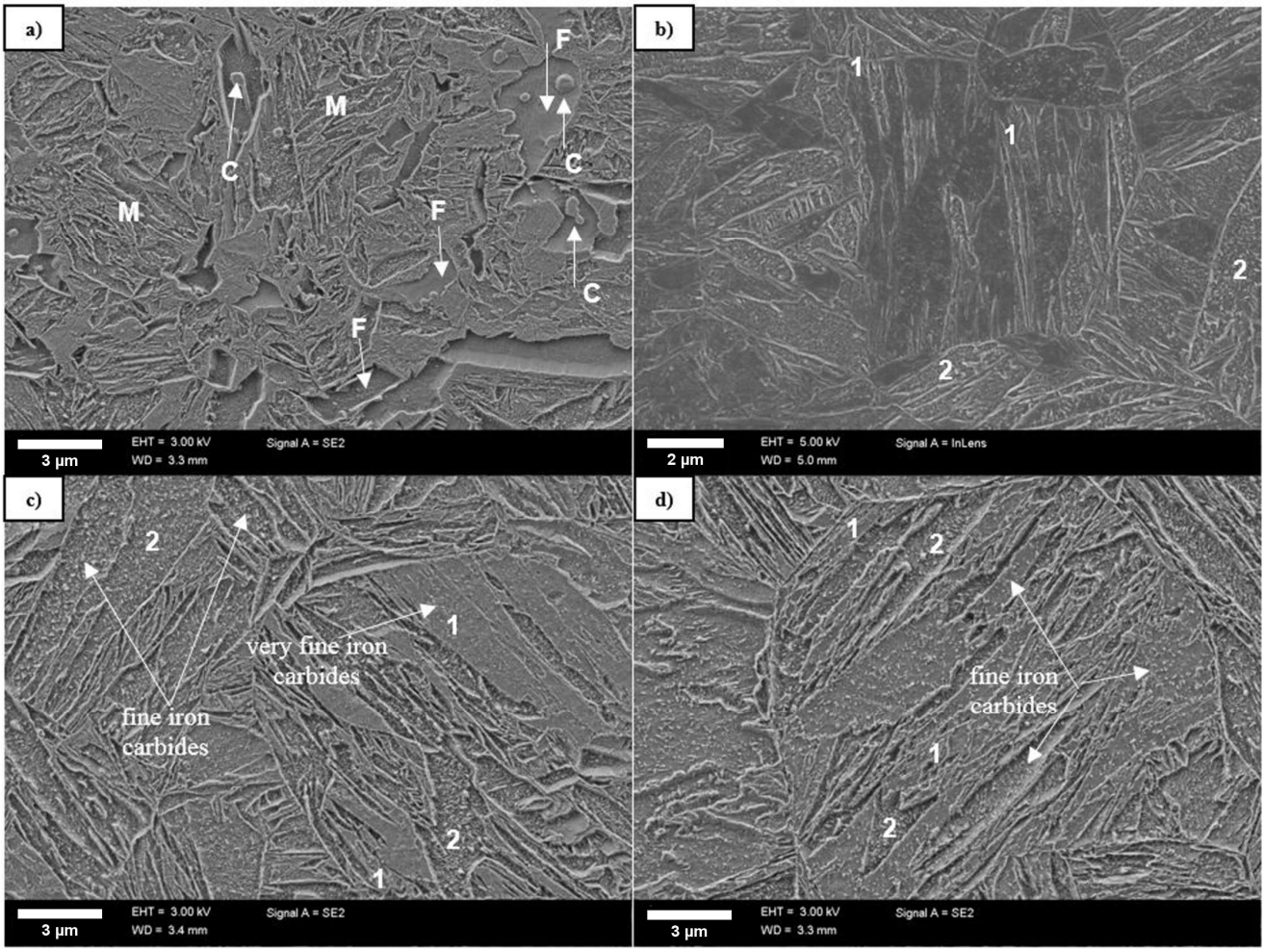

Fig. 3. (4) Example SEM micrographs of; a) 1-BA (180 s/900 °C - PH) showing undissolved cementite (C) and ferrite islands (F) in martensitic matrix (M); b) 1-BA (450 s/900 °C - PH) consisting of fresh martensite (1) and auto-tempered martensite (2); c) 1-FH (450 s/900 °C-PH) showing fine iron carbides within laths of auto-tempered martensite (2); d) 1-FH-(450 s/900 °C - PH+BH) showing iron carbides recognizable in both laths of fresh martensite (1) and areas of auto-tempered martensite (2).

Fig. 4 shows TEM analyses of extraction replica samples for micro-alloyed steel 3-CA_3. Investigations carried out for this steel revealed the presence of carbides in the size of 10–80 nm by diameter in both PH and PH+BH conditions (Fig. 4a). The analysis indicated that the carbides were relatively evenly distributed in the microstructure. The SAED patterns and EDS analysis carried out for individual carbides indicate that the dispersed precipitates are niobium rich mixture carbides (Nb, Ti)C. Example TEM image and SAED pattern of the carbide are presented in Fig. 4b. The structure of the carbides is a cubic

rock salt structure (International Centre for Diffraction Data (ICDD), 2015, space group $Fm\bar{3}m$, agreeing with the study carried out by Wu et al. (2015).

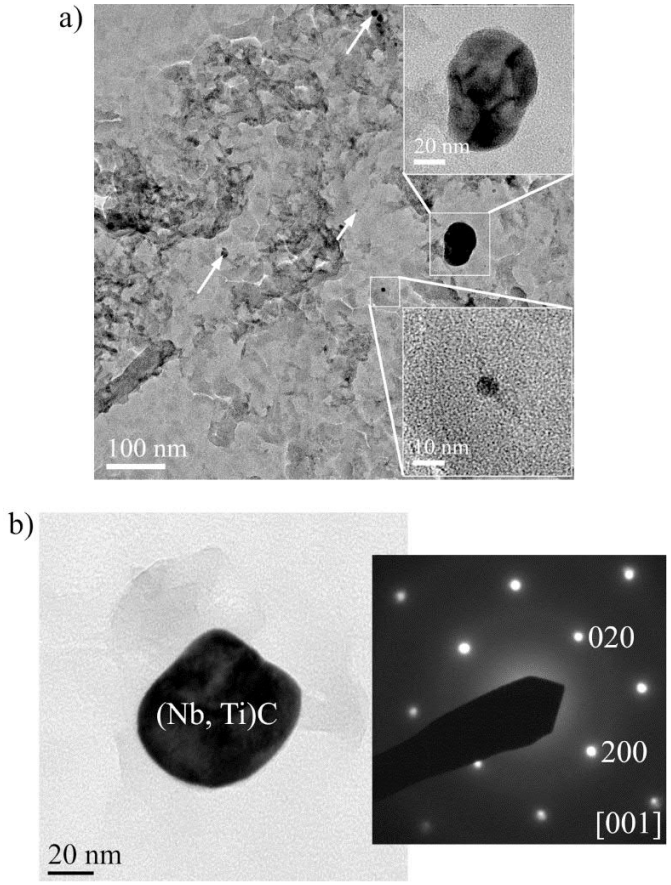

Fig. 4. TEM analyses for extraction replica samples from the micro-alloyed steel 3-CA_3; a) example extraction replica TEM-micrograph showing carbides with different sizes, some of carbides marked with arrows and higher magnification images of the small and large carbides as insets; b) TEM-micrograph and SAED-pattern for the large (Nb, Ti)C carbide indicating cubic rock salt structure.

3.2 PRIOR AUSTENITE GRAIN SIZES

Reconstructed prior austenite grain boundary maps (175 x 125 µm), viewed transverse to the rolling direction of as-received materials, are shown in Fig. 5 and Fig. 6. Prior austenite grain boundaries (PAGB) are superimposed on EBSD band contrast images as black lines. The red and green lines show packet and block boundaries of martensite, respectively.

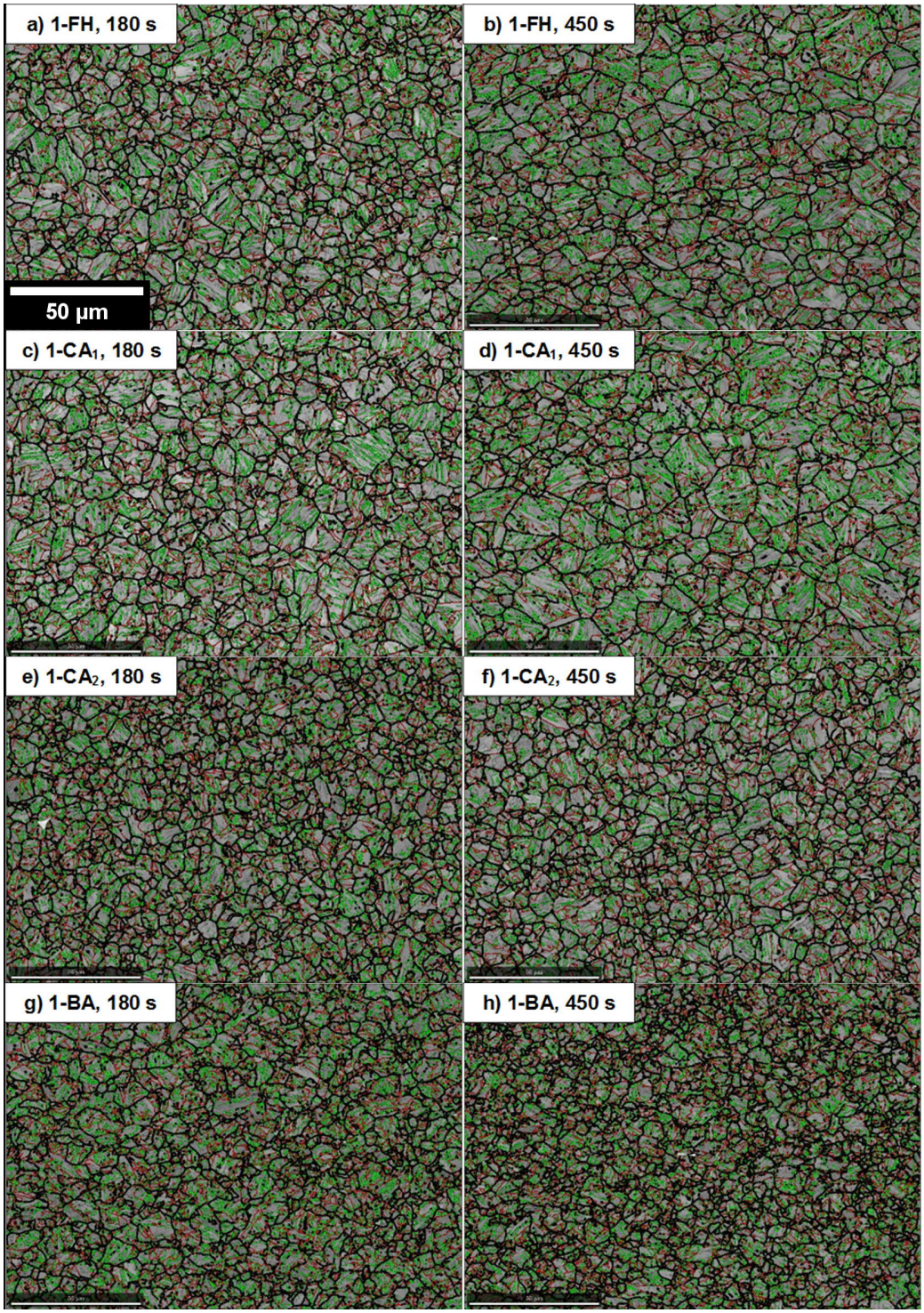

Fig. 5. (5) Prior austenite grain boundary (PAGB) maps for the steels 1-FH, 1-CA_1, 1-CA_2, and 1-BA austenitized for 180 and 450 s at 900 °C. The viewing direction is transverse to the rolling direction. PAGB are superimposed on EBSD band contrast images as black lines. The red and green lines show packet and block boundaries of martensite, respectively. The scale bar is 50 um in all images. For colors, please refer to the online version.

The reconstructed prior austenite grain boundary maps of the conventional 22MnB5 grades reveal relatively equiaxed grain morphologies (Fig. 5). The prior cold working of the 1-FH could be inherited to some extent after a typical press hardening process, however, no significant indications of the pancaked prior austenite grains can be seen. Evidently, the subsequently carried out annealing cycles have mostly eliminated the effect of earlier cold working in the case of 1-CA_1, 1-CA_2, and 1-BA. More importantly, clear differences in PAGS can be observed between the examined austenitization times (180 s and 450 s), but also between the investigated 22MnB5 steels (Fig. 5). The heating rates typical to the press hardening process increase the A_{c3} temperature of 22MnB5 grades up to around 830 °C (Nishibata and Kojima, 2013), which is notably higher than the calculated values expressed in Table 1. The grain growth of the 22MnB5 grades occurring at 900 °C is only moderate due to relatively high A_{c3}.

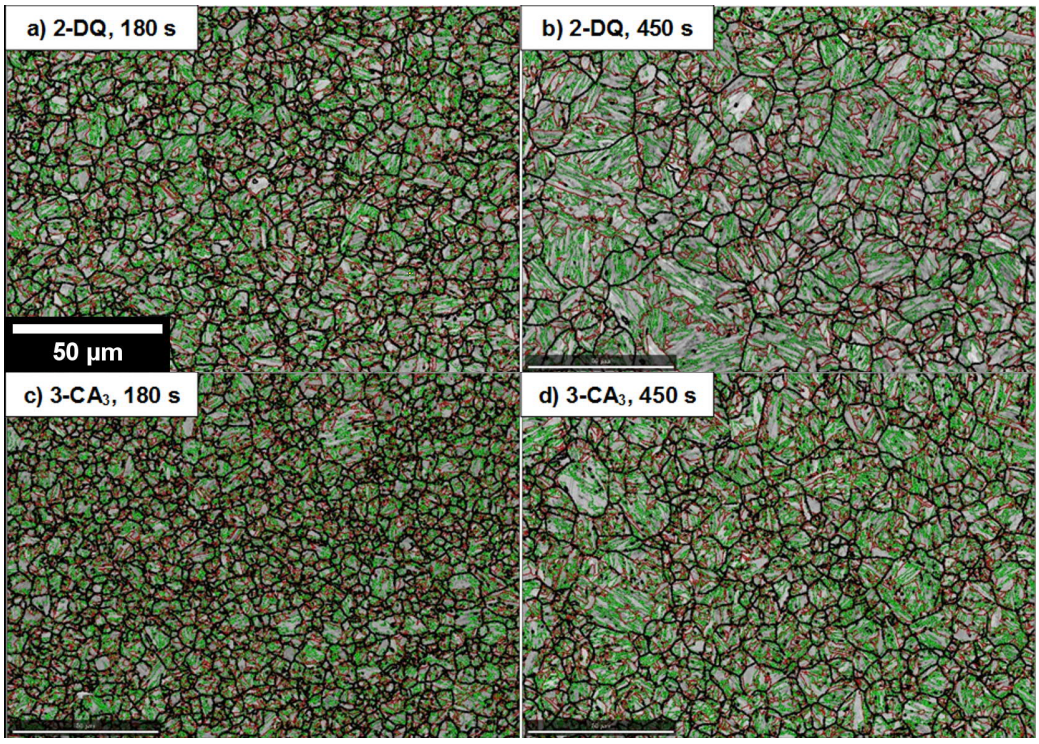

Fig. 6. (5) Prior austenite grain boundary (PAGB) maps for the steels 2-DQ and 3-CA_3 austenitized for 180 and 450 s at 900 °C. The viewing direction is transverse to the rolling direction. PAGB are superimposed on EBSD band contrast images as black lines. The red and green lines show packet and block boundaries of martensite, respectively. The scale bar is 50 um in all images. For colors, please refer to the online version.

A comparison between the prior austenite grain boundary maps presented in Fig. 5 and Fig. 6 implies that the increase in PAGS, identifiable between 180 s and 450 s austenitization times, is higher for the steels with higher carbon contents, i.e., for

the 2-DQ and 3-CA_3. Those steels show some very large prior austenite grains after 450 s austenitization (Fig. 6b and 6d). Higher carbon content naturally decreases the A_{c3} temperature, thus increasing the driving force required for the grain growth at 900 °C. A summary of the PAGS measurements is presented in Table 2. The data includes the measurement results for both transverse (TD) and longitudinal (RD) directions in relation to rolling direction of as-received materials.

Table 2. (12) The measurement results of PAGS for the PH samples austenitized for 180 and 450 s at 900 °C: TD=transverse direction, RD=longitudinal direction, i.e., rolling direction. Designation ΔGS refers to the measured grain size differences between the studied austenitization times of 450 s and 180 s.

Steel	PAGS (µm) - TD 180 s/900 °C	PAGS (µm) - TD 450 s/900 °C	ΔGS(µm) TD	PAGS (µm) - RD 180 s/900 °C	PAGS (µm) - RD 450 s/900 °C	ΔGS(µm) RD
1-FH	6.3 (±0.9)	7.5 (±1.2)	1.2	6.4 (±0.7)	9.4 (±1.3)	3.0
1-CA_1	7.3 (±0.9)	9.1 (±1.5)	1.8	7.9 (±1.1)	11.5 (±3.1)	3.6
1-CA_2	5.3 (±0.4)	5.7 (±0.7)	0.4	5.0 (±0.5)	6.1 (±0.8)	1.1
1-BA	5.3 (±0.4)	4.6 (±0.6)	-0.7	4.9 (±0.6)	4.9 (±0.8)	0
2-DQ	5.8 (±0.5)	10.4 (±1.8)	4.6	6.1 (±0.5)	11.6 (±2.7)	5.5
3-CA_3	4.6 (±0.4)	7.6 (±1.1)	3.0	4.2 (±0.4)	5.9 (±0.8)	1.7

The measured PAGS values (Table 2), show scatter between transverse and longitudinal directions in relation to the original rolling direction. This is most likely caused by the natural grain size distribution, but can be also related to the measurement direction used in the mean linear intercept method. The mean linear intercepts were measured to the vertical direction, which was parallel to the normal of the rolling direction. However, the steels that were most susceptible to the grain growth at the studied austenitization temperature of 900 °C can be identified: steels 1-FH and 1-CA_1 show higher grain growth in comparison with 1-CA_2 and 1-BA. As discussed above, a significant grain growth was also observed for the steels with higher carbon contents, i.e., for the 2-DQ and 3-CA_3.

3.3 MECHANICAL PROPERTIES AND FRACTURE BEHAVIOR

Tensile testing at a quasistatic strain-rate of $5 \times 10^{-4} s^{-1}$ was carried out for the specimens in both PH and PH+BH conditions. Fig. 7 summarizes representative examples of engineering stress-strain curves for both conditions. The curves of 1-CA_1 and 1-CA_2 are omitted for clarity.

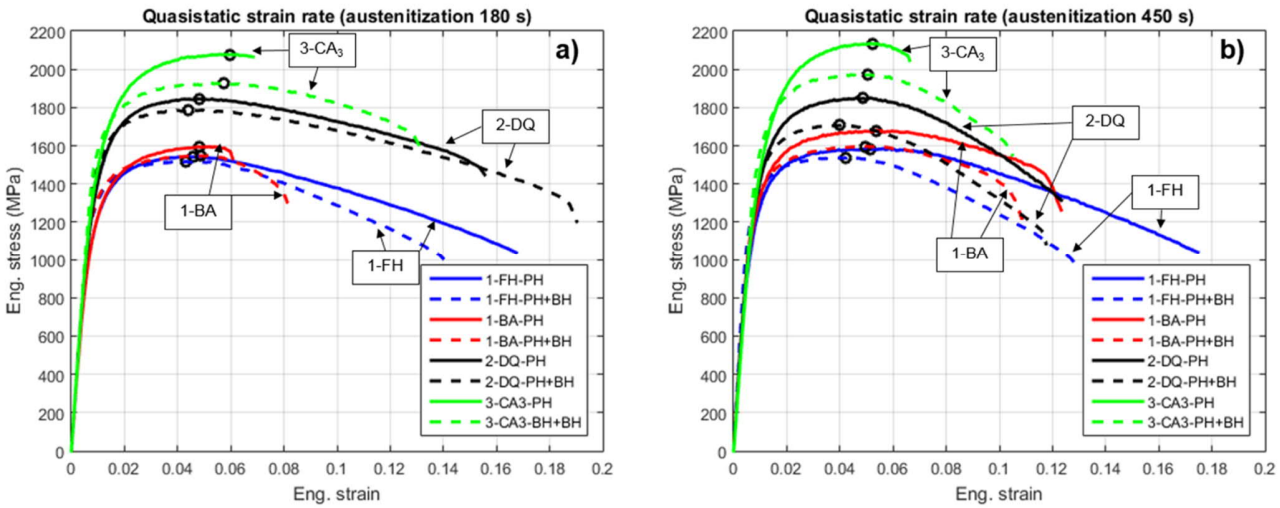

Fig. 7. Representative engineering stress-strain curves measured at a quasistatic strain-rate of 5 x $10^{-4}s^{-1}$ for; a) PH and PH+BH materials austenitized for 180 s at 900°C; b) PH and PH+BH materials austenitized for 450 s at 900°C. The highest points of the curves, indicating on the ultimate tensile strength and uniform elongation, are marked with unfilled dots. The curves of 1-CA_1 and 1-CA_2 are omitted for clarity.

As can be seen in Fig. 7, the samples tested in the PH+BH condition show higher 0.2 % proof stress ($R_{p0.2}$) values in comparison with the PH condition. In general, the ultimate tensile strength (R_m) decreases in baking and uniform elongation (A_g) shows a minor decrease, respectively. The stress-strain curves presented in Fig. 7a and 7b also indicate that baking increases the post-uniform elongation of the 3-CA_3. Similar behavior, albeit less significant, can be observed for the 1-BA and 2-DQ austenitized for 180 s. However, this behavior does not seem to be present in the case of longer austenitization time of 450 s.

Fig. 8 shows SEM images of the fracture surfaces of selected tensile test specimens in both PH and PH+BH conditions austenitized for 180 s at 900 °C. The specimens were observed from the middle parts of the fractured sections. The specimens analyzed correspond to the same specimens as the representative stress-strain curves presented in Fig. 7a.

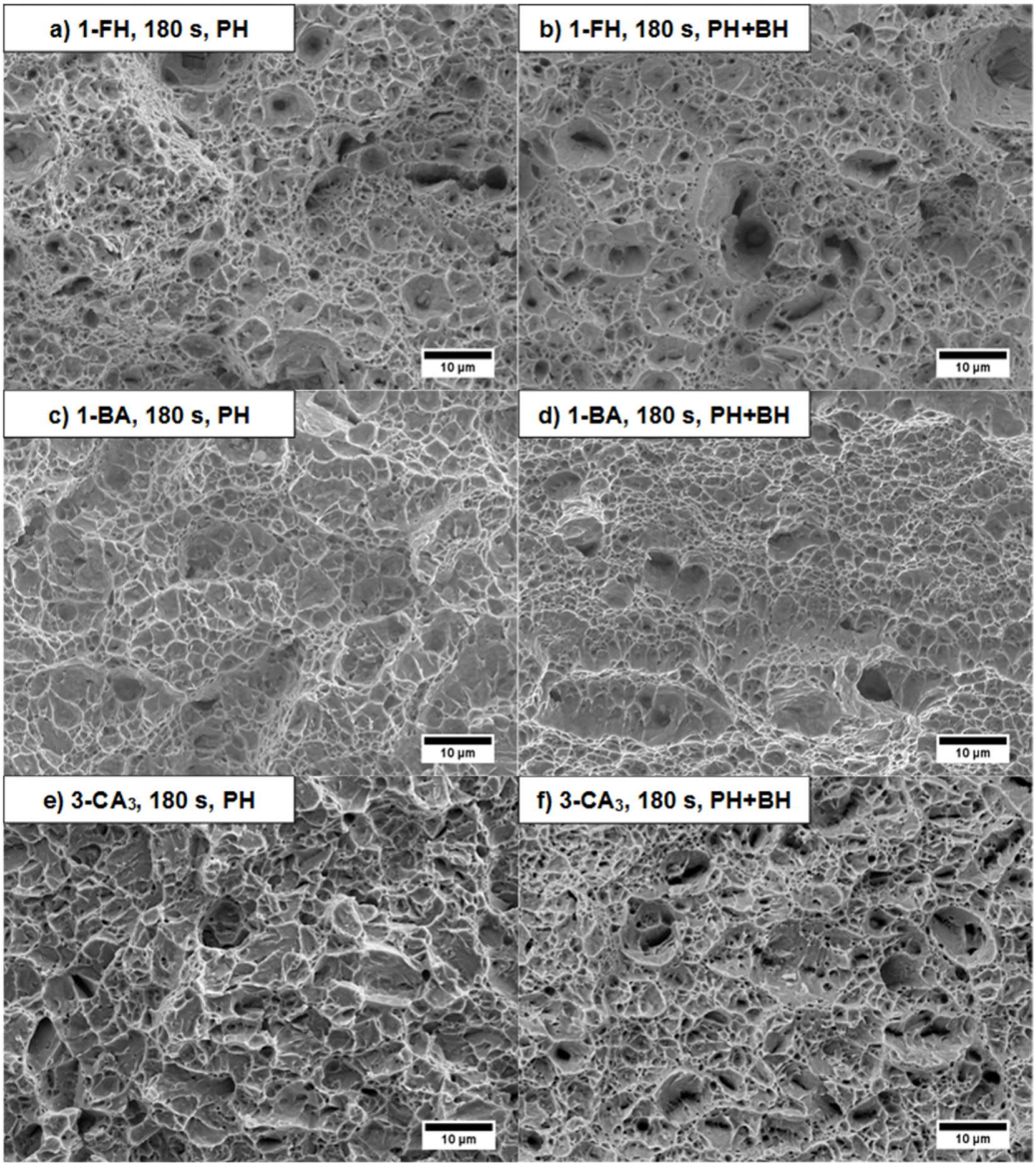

Fig. 8. SEM images of the fracture surfaces of selected tensile specimens for steels 1-FH, 1-BA, and 3-CA_3 austenitized for 180 s at 900 ˚C.

As can be seen (Fig. 8), the fracture surfaces are typical for medium-carbon (0.23–0.35 % C) martensitic steels. However, clear differences between steels 1-FH, 1-BA and 3-CA_3 with different carbon contents can be observed. The fracture surfaces of the 1-FH (Fig. 8a and 8b) represent a typical ductile fracture of martensite with a number of micro-voids and ductile dimples. A relatively large number of micro voids is in line with a large post-uniform elongation seen in Fig. 7a. In addition, the ductile fracture of the 1-FH has led to a highly but uniformly strain hardened matrix and the formation of relatively large cavities due to the presence of hard second phase particles. The fracture surfaces of the 1-FH do not reveal significant differences

between the PH and PH+BH conditions, thus suggesting that the baking do not cause remarkable changes in elongation behavior of the 1-FH. Fig. 8b and 8c represent the fracture surfaces of the 1-BA. In the PH condition (Fig. 8c) there exists some cleavage facets, which is an indication of reduced post-uniform elongation. In addition, the dimples of the matrix are relatively shallow and the number of deep micro voids is clearly smaller in comparison with the ones observed for the 1-FH. However, there do not either exist significant differences between the fracture surfaces observed in the PH (Fig. 8c) and PH+BH (Fig. 8d) conditions of the 1-BA. The fracture surface of the 3-CA_3 (Fig. 8e), in turn, indicates on the reduced ductility. Accordingly, the number of cleavage facets is clearly the largest. However, in the PH+BH condition (Fig. 8f), the fracture surface of the 3-CA_3 shows highly elongated dimples and actually resembles much of the fracture surfaces of the 1-FH (Fig. 8a and 8b).

Table 3 shows a summarization of the mechanical properties. In addition, micro hardness values in the PH condition and phases present after the die quenching step are presented. In the case of tensile properties, the expressed values are averages of three (450 s/900 °C) or two repetition tests (180 s/900 °C).

Table 3. Tensile test results for PH and PH+BH samples at a quasistatic strain-rate of 5×10^{-4} s^{-1}. Microhardnesses (HV 0.5 kg) were measured only for the samples in the PH condition. RA in the "Phases" column refers to the slightly higher amount of retained austenite observed in the EBSD analysis. In the "Phases" column, F refers to ferrite islands and C to the undissolved cementite, respectively.

	180 s/900 °C - PH					180 s/900 °C - PH+BH				
Steel	**$R_{p0.2}$ (MPa)**	**R_m (MPa)**	**$R_{p0.2}/R_m$**	**A_g (%)**	**HV 0.5 kg**	**$R_{p0.2}$ (MPa)**	**R_m (MPa)**	**$R_{p0.2}/R_m$**	**A_g (%)**	**Phases**
1-FH	1110	1550	0.72	4.6	490 ± 18	1240	1510	0.82	4.1	M
1-CA_1	1130	1570	0.72	4.3	490 ± 19	1240	1520	0.82	4.1	M
1-CA_2	1150	1590	0.72	4.4	498 ± 11	1300	1550	0.84	4.0	M
1-BA	1130	1610	0.70	4.8	504 ± 15	1270	1540	0.82	4.6	M+F+C
2-DQ	1280	1810	0.71	5.0	544 ± 11	1420	1750	0.81	4.9	M
3-CA_3	1430	2080	0.69	5.4	643 ± 14	1580	1930	0.82	5.6	M+RA

	450 s/900 °C - PH					450 s/900 °C - PH+BH				
Steel	**$R_{p0.2}$ (MPa)**	**R_m (MPa)**	**$R_{p0.2}/R_m$**	**A_g (%)**	**HV 0.5 kg**	**$R_{p0.2}$ (MPa)**	**R_m (MPa)**	**$R_{p0.2}/R_m$**	**A_g (%)**	**Phases**
1-FH	1130	1560	0.72	5.0	482 ± 6	1240	1530	0.81	4.4	M
1-CA_1	1120	1550	0.72	4.5	487 ± 3	1200	1490	0.81	4.0	M
1-CA_2	1160	1610	0.72	4.3	494 ± 8	1280	1540	0.83	3.8	M
1-BA	1170	1650	0.71	5.4	517 ± 8	1290	1520	0.81	4.9	M
2-DQ	1260	1810	0.70	4.8	536 ± 6	1340	1690	0.79	4.1	M
3-CA_3	1410	2090	0.67	5.3	638 ± 10	1570	1950	0.80	5.0	M+RA

The data presented in Table 3 proposes that the steels tested in the PH condition show generally slightly higher A_g as the strength level of steel is increased with a higher carbon content. However, the differences are relatively small. The measured micro hardness values are in a good agreement with the tensile properties. A yield to tensile ratio, i.e., $R_{p0.2}/R_m$ is expressed here to estimate the fraction of softer and harder elements in the microstructure. This is based on the assumption that softer elements yield at lower strength levels and have larger ability to deform plastically before necking. (14) In the present study (17), the ratio (14) can be used to indicate the fraction of auto-tempered martensite and other softer phases such as ferrite and retained austenite. The $R_{p0.2}/R_m$ ratios of the 2-DQ are slightly smaller than the $R_{p0.2}/R_m$ ratios of the 22MnB5 grades. This may be a result of enhanced auto-tempering which may have been promoted during the die quenching of thicker, 2.3 mm thick samples of the 2-DQ. In the case of the1-BA, the presence of ferrite islands was observed after the shorter austenitization time of 180 s. This finding may be used to explain smaller $R_{p0.2}/R_m$ ratio of 0.70 measured for the 1-BA, when comparing to results of the other 22MnB5 grades showing $R_{p0.2}/R_m$ ratios of 0.72. In addition, the EBSD investigations revealed small amounts of retained austenite (<1.0 %) especially for the 3-CA_3: the obtained $R_{p0.2}/R_m$ ratios of 0.69 (180 s) and 0.67 (450 s) are in agreement with that finding.

Fig. 9 uncouples the effect of baking treatment (170 °C/20 min) on the mechanical properties of press hardened steels indicated with $\Delta R_{p0.2}$, ΔR_m, and ΔA_g.

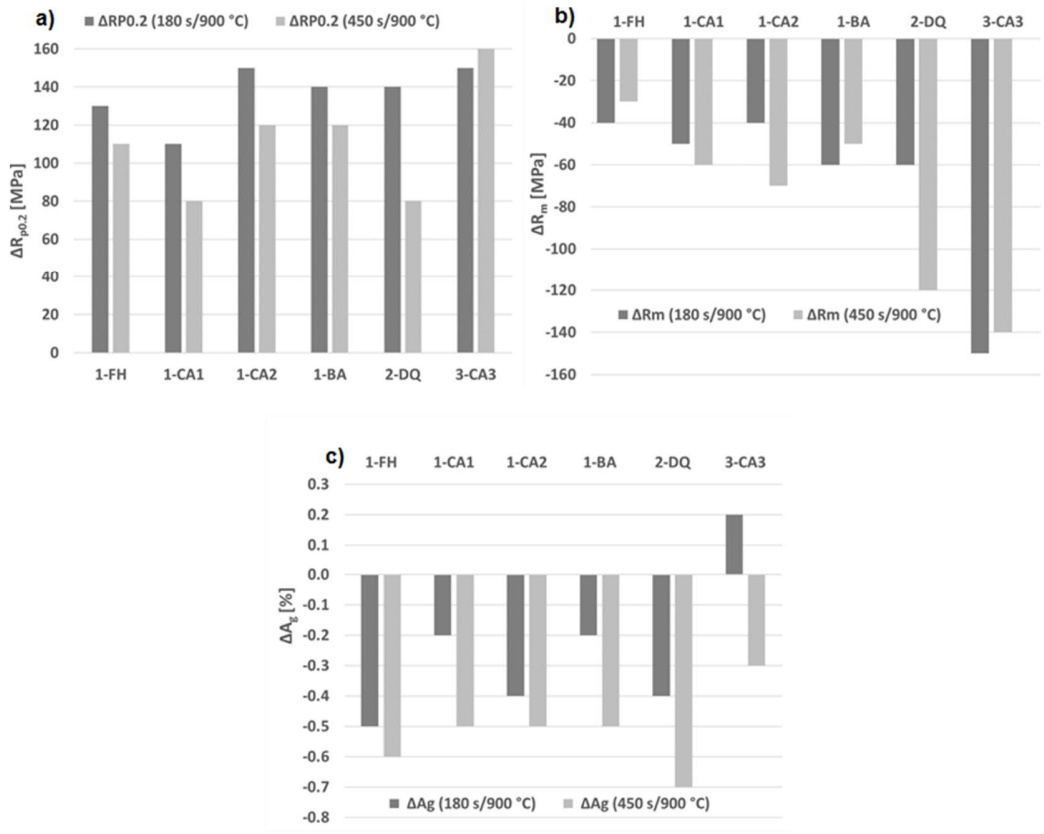

Fig. 9. Summarized effect of baking treatment (170 °C/20 min) on the mechanical properties of press hardened steels 1-FH, 1-CA_1, 1-CA_2, 1-BA, 2-DQ, and 3-CA_3; a) $\Delta R_{p0.2}$; b) ΔR_m; c) ΔA_g.

Fig. 9a implies that the determined BH effect, in terms of $\Delta R_{p0.2}$, is between 80 and 160 MPa. The 3-CA_3 exhibits the strongest BH effect of 150 and 160 MPa, while the $\Delta R_{p0.2}$ values of the 1-CA_1, 110 and 80 MPa, are the smallest. It can be also noticed that the BH effect is generally higher for the shorter austenitization time of 180 s. However, the behavior of the 3-CA_3 is different to the others, since it do not exhibit higher $\Delta R_{p0.2}$ for 180 s austenitization time. As can be seen in Fig. 9b, the resulting decrease in tensile strength R_m seems to be higher for the steels 2-DQ and 3-CA_3 with higher carbon contents. However, the results of the 2-DQ, austenitized for 180 s, do not seem to fit this trend: the ΔR_m value is at the same level (around 50 MPa) with the 22MnB5 grades. In the case of 450 s austenitization, the observed change in A_g is around 0.5 % for the steels 1-FH, 1-CA_1, 1-CA_2, 1-BA and 2-DQ. The shorter austenitization time of 180 s, in turn, resulted in slightly smaller decrease

in A_g. The 3-CA_3 exhibited somewhat exceptional behavior and showed slightly smaller ΔA_g for 450 s austenitization time and actually a minor increase in A_g in the case of 180 s, respectively.

4. DISCUSSION

4.1. (2) ROLE OF IRON CARBIDE PRECIPITATION IN THE BH EFFECT OF PHS

The formation of auto-tempered martensite is characteristic to die quenching (Matsuda et al., 2013) and is enhanced by relatively high transformation temperatures of PHS. M_s and M_f temperatures settle around 400 °C and 200 °C as noted for example by Nishibata and Kojima (2013). The quenching conditions of the present study (Fig. 2a) resulted in a corresponding auto-tempering behavior. The same behavior was observed for all investigated steels of 22MnB5, 30MnB5 and 34MnB5 types. The auto-tempering process resulted in the formation of fine iron carbides within martensite laths during die quenching, i.e., the fine carbides were present within the laths of auto-tempered martensite in the PH condition (Fig. 3c). This result is supported by the findings of Choi et al. (2015). Hutchinson et al. (2011) studied martensitic C-Mn steels with a range of carbon contents (0.1–0.5 C %) and showed that most of the carbon can segregate to the dislocations cores of martensite laths and packets already during quenching. The same observation was made in the study of and Sulistiyo et al. (2016) for a PHS with a carbon content of 0.31 %. According to these findings, the Cottrell atmosphere formation can take place already during quenching of PHS. As already discussed above, it is unlikely that Cottrell atmosphere formation and resulting dislocation locking is responsible for the observed BH effect of martensitic steels. In turn, it seems evident that dislocation locking occurs very fast during quenching step. This is because the martensitic phase transformation should lead to the formation of high amount of fresh dislocations prior to auto-tempering effects. According to Sulistiyo et al. (2016), the baking treatment actually leads to the saturation of Cottrell atmospheres and reduction of solute carbon content due to progressive precipitation of transition carbides. The SEM observations of the present study support this idea: the more progressed precipitation of fine iron carbides was observed in the PH+BH condition (Fig. 3d). To compare, the microstructure obtained in the PH condition revealed carbides generated during auto-tempering (Fig. 3c), but clearly smaller density of precipitates within fresh martensite laths. To sum up above, both auto-tempering and baking treatment can cause precipitation of fine iron carbides in press hardening steels of 22MnB5, 30MnB5, and 34MnB5.

According to Krauss (1995), the precipitation of transition carbides occurs in the interiors of martensite laths. Thus, the precipitation of fine carbides can refine the microstructure by decreasing the mean free path of dislocation glide. As noted by (Kuhlmann-Wilsdorf, 1989), fine carbides can act as non-shearable particles and effectively increase the strain hardening rate of martensite crystals. According to this theory, the key strengthening mechanism of bake hardened martensitic steels is the strain hardening provided by the interactions been transition carbides and already existing dislocation substructures. As noted by Krauss (1995), higher carbon content results in a higher density of transition carbides and a stronger reduction in dislocation glide distances. Therefore, higher carbon content finally results in higher stress required for dislocation movement, thus increasing yield strength of martensitic steel. Our present results support this theory: the attained increase in $R_{p0.2}$ was largest for the 3-CA_3 steel with the highest carbon content of 0.35 % (Fig. 9a). However, the differences in $\Delta R_{p0.2}$ values were relatively small among the investigated steels. The apparent scatter of the measured BH effect (Fig. 9a) is probably mostly contributed to the measured differences in PAGS (Table 2). This notation can be explained according to the study carried out by Kennett et al. (2015). The scientists reported that the smaller PAGS could also increase the dislocation density of the transformed martensite by increasing the grain boundary area of martensitic steel. Thus, smaller PAGS can also enhance the interactions between transition carbides and dislocation substructures, and thus influence the BH response of PHS.

According to Krauss (1995), the precipitation of fine iron carbides consumes solute carbon and thus, the lattice strains of tetragonal martensite are decreased in LTT processes such as during the paint baking cycle of 170 ˚C/20 min. The softening of martensite occurring in the baking process can be evaluated by comparing the ultimate tensile strength values. Our results (Fig. 9b) show a clear decrease in R_m values due to baking. Hutchinson et al. (2015) reported similar results for martensitic C-Mn steels, tempered at 200 ℃ for 3 minutes. Since the tensile strength of as-quenched martensite is strongly contributed to the amount of carbon (Krauss, 1999), it can be expected that higher carbon content of steel leads to the higher decrease in tensile strength during the paint baking. The present study support this assumption: the obtained decrease in ΔR_m is highest (around 150 MPa) for the 3-CA_3 with the highest carbon content of 0.35 %. The ΔR_m is about three times higher in comparison with the 22MnB5 grades 1-FH, 1-CA_1, 1-CA_2, and 1-BA. However, Hutchinson et al. (2011) observed that the amount of free carbon were actually almost equivalent, only around 0.02 %, for the martensitic steels with various carbon contents of 0.1–0.5 %. This finding indicates that the strength of martensite is not after all provided by traditional solid solution strengthening. In turn, the scientists pointed out that the tensile strength of as-quenched martensite is strongly contributed to the amount of segregates generated at lath boundaries and dislocations during quenching. According to Hutchinson et al. (2011),

the density of these carbon-enriched segregates was higher in the steels with higher carbon contents. This finding can be used to explain our present results: the stronger decrease in R_m is connected with the stronger segregation of carbon atoms from Cottrell atmospheres towards fine iron carbides. Consequently, higher carbon content leads to the stronger precipitation and larger decrease in R_m.

However, the measured ΔR_m values of the 2-DQ did not entirely fit the above-discussed trend. For the 2-DQ a decrease of only 60 MPa was observed in the case of shorter austenitization time of 180 s (Fig. 9b). Taking into account a relatively high carbon content of 0.29 %, the more expected decrease in R_m would be around 100–120 MPa. In turn, the longer austenitization cycle of 450 s resulted in more expected tensile strength decrease of 120 MPa. That value is significantly higher in comparison with the investigated 22MnB5 grades, all of which showed almost a constant decrease of about 50 MPa in the case of both austenitization times. As indicated in Table 2, the 2-DQ steel had a higher chromium content (0.66 %) than the other investigated steels (0.2–0.3 %). Some earlier findings can be used to evaluate the observed BH behavior of the 2-DQ steel. Pereloma et al. (2012) have suggested that higher chromium content of steel reduces the level of solute carbon, and thus slows down the static strain aging of low carbon steels. The results more applicable to our study has been reported by Otani et al. (2015). The scientists measured smaller solute carbon contents for a press hardened steel of 34CrB5 type (0.2 % Mn), with exceptionally high chromium content of 1.2 %, austenitized for 360 s at 900 ˚C. They also observed that the tensile strength of the 34CrB5 was higher than 34MnB5 after LTT. Accordingly, the 2-DQ would have contained a smaller amount of carbon contributing to the transformation strengthening, but also contributing to the softening process of the martensitic matrix occurring during baking. As indicated in Table 3, the tensile strength of the 2-DQ is the same, 1810 MPa, for both austenitization times. However, the yield strength is higher for the shorter austenitization time of 180 s, probably due to smaller PAGS. This result implies that the strengthening effect provided by carbon atoms segregated to the lath boundaries, being mainly responsible for the tensile strength of martensite, is slightly smaller in case of 180 s austenitized samples. A clearly larger ΔR_m determined for the longer austenitization time of 450 s, indicates that the amount of carbon available for the strengthening was higher. Consequently, the baking treatment has led to a larger decrease in R_m. Pereloma et al. (2012) have also suggested that chromium can chemically stabilize iron carbides by the mechanism referred to as chromium enrichment. According to this, the longer austenitization time of 450 s was required to dissolve all iron carbides formed during the direct quenching of the 2-DQ. In other words, a higher amount of carbon was released back to the solid solution during the longer austenitization cycle.

4.2. (2) CORRELATION BETWEEN PAGS AND BH EFFECT OF PHS

As demonstrated for example by Morito et al. (2006), martensite tends to form a hierarchical structure consisting of packets, blocks and laths. The results gathered by Galindo-Nava and Rivera-Díaz-del-Castillo (2015) strongly suggest that PAGS correlates linearly with packet and block sizes of martensite. Therefore, PAGS can be reliably used as a demonstrative grain size indicator of martensitic microstructures. In the present (17) study, the reconstructed PAGB maps (Fig. 5 and Fig. 6) were used in order to evaluate the grain size effects in the bake hardening behavior of PHS. A comparison between the investigated austenitization cycles of 180 and 450 s at 900 °C and corresponding PAGS (Table 2) allows uncoupling the grain size effect within each specific chemical composition. The results summarized in Fig. 9a show a clear correlation between the shorter austenitization cycle, 180 s/900 °C, (smaller PAGS) and higher $\Delta R_{p0.2}$ for the steels 1-FH, 1-CA_1, 1-CA_2, 1-BA, and 2-DQ. The shorter austenitization time of 180 s resulted in the yield strength increase of 140 MPa on average. The longer austenitization time of 450 s led to average increase of only around 110 MPa. This result indicates that there clearly exists a correlation between PAGS and BH effect in terms of $R_{p0.2}$. In fact, the effect of PAGS has been probably slightly decreased by the presence of small amount of retained austenite or undissolved cementite, both of which are promoted by the shorter austenitization times. The micro-alloyed steel 3-CA_3 was the only exception in the observed trend (Fig. 9a) and exhibited almost a constant increase in $R_{p0.2}$ for both austenitization times. This result may be related to the observed presence of mixture carbides of (Nb, Ti)C with a cubic rock salt structure (Fig. 4). The carbides of this type, if evenly distributed in the microstructure, may shorten the mean free distance of dislocation motion along with fine iron based carbides. (15) The presence of additional carbides may thus reduce the significance of PAGS, which can also contributes to the interactions and dislocation glide distances as discussed above.

Despite the observed correlation between PAGS and measured increase in yield strength values, the results of the present study do not show a clear dependency between PAGS (Table 2) and measured ΔR_m values (Fig. 9b). Morito et al. (2006) reported that the PAGS did not significantly correlate with the lath size of martensite in Fe-0.2 C and Fe-0.2C-2Mn steels. Zhang et al. (2012) reported similar results for a 25CrMo48V steel. These findings, combined with the current understanding of the carbon segregation and dislocation locking occurring during quenching at lath boundaries (Hutchinson et al., 2011), can be used to explain the present results. Baking leads to the diffusion of carbon atoms from lath boundaries towards lath interiors, acting as nucleation sites for transition carbides (Krauss, 1995). Therefore, the diffusion distances between are practically of the same magnitude despite the measured differences in PAGS. No correlation between PAGS (Table 2) and measured ΔA_g (Fig. 9c) was either observed, albeit the obtained decrease in A_g was slightly higher in the case of 450 s austenitization, i.e., in the case of larger PAGS. However, we believe that the observed behavior is rather associated with more inhomogeneous microstructure resulting in the shorter austenitization cycle of 180 s/900 °C. For example, the presence of ferrite or retained austenite can have a small effect on the measured A_g values.

4.3. (2) **EFFECT OF PAINT BAKING TREATMENT ON THE STRESS-STRAIN BEHAVIOR OF PHS**

The stress-strain curves measured for the samples in both PH and PH+BH conditions (Fig. 7) showed continuous yielding throughout the quasistatic tensile test, i.e., elevated yield point did not appear either after the baking treatment. The continuous yielding and low elastic limits are typical to martensitic steels and have been addressed for example by Hutchinson et al. (2015) As discussed by Sulistiyo et al. (2016), the continuous yielding of bake hardened PHS could be explained by the presence of significant amount of mobile dislocations. However, the earlier discoveries on the dislocation pinning effect, occurring already during quenching (Choi et al., 2015), argues against this interpretation. Hence, there is a reason to believe that continuous yielding and low elastic limits are involved with other phenomena characteristic to martensitic microstructures. One considerable mechanism explaining the stress-strain behavior of martensitic steels have been addressed in a recent study of Hutchinson et al. (2015). The scientists have highlighted the role of internal intra-granular stresses in the mechanical behavior of as-quenched martensitic steel sheets. According to Hutchinson et al. (2015), the martensite that is formed in thin steel sheets is most importantly involved with short-distance residual stresses, which may have either favorable or unfavorable direction in relation to the external loading direction. Accordingly, a part of these intra-granular internal stresses may act to the same direction with the external load, and thus assist in yielding already at low load levels. This interpretation can be largely used to explain the stress-strain behavior typical to both as-quenched and LTT martensites. In the present study, this theory is applicable to explain the smooth and rounded form of stress-strain curves attained on both PH and PH+BH steels

(Fig. 7). More importantly, the BH effect determined in terms of $\Delta R_{p0.2}$ can be also connected with the same theory. The residual stresses assisting the local yielding at low stress levels are constantly reduced during baking. This results in higher 0.2 % proof stress when the material is tensile tested after baking.

As discussed by Hutchinson et al. (2015) the relaxation of internal stresses reduces the amount of strain needed to reach instability in a tensile test, thus reducing the uniform elongation of LTT treated martensites. In the present study the baking treatment of 170 °C/20 min resulted in the decrease in A_g for the investigated steels 1-FH, 1-CA_1, 1-CA_2, 1-BA, and 2-DQ (Fig. 9c). The measured decrease of approximately 0.5 % on average was observed for the longer austenitization time of 450 s, whereas 180 s austenitized samples showed more scatter and slightly smaller decrease in A_g. Hutchinson et al. (2015) reported a corresponding decrease of about 0.5 % after low-temperature tempering at 200 °C for 3 min. Their material model and earlier results of Saeglitz and Krauss (1997) support the trend of ΔA_g observed in the present study. The attained decrease in uniform elongation suggests that iron carbide formation and higher strain hardening rate of the PH+BH treated martensite lead to the earlier instability in tensile deformation. This in turn, resulted in the decreased uniform elongation and earlier on-set of necking in tensile test. The larger scatter in ΔA_g was observed in the case of shorter austenitization time of 180 s. This may be also a result of inhomogeneous microstructure.

Steel 3-CA_3 showed somewhat different BH behavior in terms of ΔA_g: the steel did not exhibit as significant changes in A_g in comparison with the other investigated steels (Fig. 9c). In fact, our results showed a small increase in A_g for 180 s austenitization at 900 °C. Because the measured differences in A_g values are relatively small, it can be thought that the result is partially caused by natural scatter. On the other hand, TEM analysis carried out for 3-CA_3 revealed the presence of niobium rich mixture carbides (Nb, Ti)C (Fig. 4). The formation of these precipitates consumes solute carbon similarly to the precipitation of iron carbides. This indicates that the amount of carbon available for further precipitation of fine iron-based carbides occurring during baking must be slightly smaller. Hutchinson et al. (2015) have suggested that the on-set of necking is avoided as long as some elements in the martensitic structure remain in elastic state. It is possible that the amount of these elastically behaving elements was higher in the 3-CA_3 steel due to the presence of additional (Nb, Ti)C precipitates which can influence the local stress fields. Accordingly, the baking-induced decrease in uniform elongation was reduced, since the relaxation of internal stresses was at least locally prevented. Therefore, additional precipitates with suitable size and distribution may have a role in preventing typically occurring decrease in uniform elongation, which was observed for the other steels under investigation.

4.4. (2) EFFECT OF PAINT BAKING ON THE DUCTILITY OF PHS

Uniform elongation is an appropriate measure of ductility, since it indicates the strain needed to cause instability in a tensile test. However, it is not the most representative measure to be used for evaluating the performance of PHS based on the conventional tensile test data. That is, the ductility of martensite has been reported (Krauss, 1995) to reduce with higher carbon contents, i.e., both necking and post-uniform elongation are reduced, but uniform elongation is increased instead. Instead, Larour et al. (2010) have suggested that the amount of post-uniform elongation indicates much better on the bendability of AHSS (Advanced High-Strength Steels), which correlates satisfactorily with the crash performance. It is still worth noting that also the value of total elongation is a sensitive measure of ductility and has been reported to show relatively large variation in particular when tensile testing martensitic PHS (Labudde and Bleck, 2009).

Our tensile test results showed that the investigated 22MnB5 grades did not exhibit significant changes in the elongation behavior due to baking (Fig. 7). There exists some differences in the measured post-uniform elongations, however, these are most likely caused by the natural scatter in the material properties, e.g., by random distribution of hard second phase particles such as TiN and MnS. The statistical distribution of second phase particles of that type is worth noting, since the cross-sectional areas of the tensile test specimens used in the present study were relatively small. The fracture surfaces of 1-FH (Fig. 8a and 8b) did not reveal significant differences between the samples of PH and PH+BH conditions, thus suggesting that the baking did not cause remarkable changes either in the ductility of 22MnB5 grades. The 1-BA exhibited exceptionally small post-uniform elongation in the case of 180 s austenitization time (Fig. 7a), whereas for 450 s (Fig. 7b) no significant differences in post-uniform elongation were seen. The fracture behavior of the 1-BA (Fig. 8c and 8d) is in line with the small post-uniform elongation values obtained for 180 s austenitized samples, and can be explained with the presence of undissolved cementite (Fig. 3a). This result implies that incomplete austenitization needs to be avoided in order to guarantee appropriate ductility of PHS. According to Saeglitz and Krauss (1997), coarse secondary phase particles have a significant role in the plastic flow after reaching the uniform elongation. In contrast, Saeglitz and Krauss (1997) have suggested that fine transition carbides precipitated during LTT are too fine to take part in the ductile fracture. The observed fracture behavior of the 1-BA supports this theory, since the measured total elongation values were clearly larger for the sample austenitized for 450 s.

The 3-CA_3 steel of 34MnB5 type exhibited very small values for post-uniform elongation in the PH condition. In addition, the fracture surface of the 3-CA_3 implied the most brittle behavior among the investigated steels in the PH condition. As reported by Saeglitz and Krauss (1997), this type of fracture behavior is an indication of high amount of pinned dislocations and is mainly caused by the high carbon content of steel. Actually, Leslie and Sober (1967) proposed that the interactions between carbon atoms and dislocations may increasingly control the mechanical behavior with the carbon contents of 0.30 % and higher. Higher carbon content of martensite naturally results in higher strain hardening rate and higher tensile strength in plastic deformation (Krauss, 1995). At very high tensile strength levels, only a small post-uniform elongation is required to generate high local stress levels required for fracture (Saeglitz and Krauss, 1997). In the case of 3-CA_3, the ultimate tensile stress level is extremely high, over 2000 MPa. After reaching the point of uniform elongation there does not practically exist any sources for plastic deformation when the steel is tested in as-quenched condition, i.e., in the PH condition. On the contrary, the ductile fracture behavior of the 1-FH (Fig. 8a), indicates that the lower ultimate tensile stress level of around 1550 MPa requires considerable necking deformation to reach critical ductile fracture stress for a given distribution of second phase particles. However, as can be seen in Fig. 8f, the subsequently carried out baking has changed the fracture behavior of the 3-CA_3 considerably towards ductile: the number of large cleavage facets has significantly decreased and the number of deep micro voids has increased, indicating on the larger post-uniform elongation. The improved fracture behavior can be explained with the earlier findings of Saeglitz and Krauss (1997) considering LTT martensites. The scientists suggested that a type of re-formation of mobile dislocations could be associated with the precipitation of transition carbides. Accordingly, carbon is removed from the Cottrell atmospheres and some dislocation segments are simultaneously free from the influence of dislocation pinning. A combination of new mobile dislocations and reduced tensile stress level seems to be of high importance in order to gain more plasticity and increase in post-uniform elongation.

When combining the observations of the present study with the current understanding of LTT treated martensitic steels, it can be suggested that a typical paint baking procedure of automotive components can be most likely used to improve fracture behavior of ultra-high strength PHS, in particular with carbon contents higher than 0.30 %. The increasing carbon content has the most important effect on the mechanical behavior of martensite, since it leads to the stronger dislocation locking, but also to the stronger precipitation of fine iron-based carbides. However, as described by Krauss (1995) and also demonstrated in the present study, there exists certain secondary factors influencing strain hardening behavior, mechanical properties and fracture behavior of PHS. These are prior austenite grain size, transition carbide/dislocation substructure, and distribution of second phase particles, all of which are influenced by steel cleanliness and austenitizing parameters.

5. CONCLUSIONS

The bake hardening (BH) behavior of press hardened boron steels (PHS) with various carbon contents was investigated. The results of the present study can be concluded as follows:

- The press hardened martensitic steels exhibited a relatively strong BH effect when they were subjected to a typical baking procedure of 170 °C/20 min.
- The investigated PHS grades of 22MnB5, 30MnB5, and 34MnB5 type showed increases in yield strength ($R_{p0.2}$) of 80–160 MPa and decreases in tensile strength (R_m) of 30–150 MPa due to baking.
- A correlation between $\Delta R_{p0.2}$ and smaller prior austenite grain size (PAGS) was observed for the investigated 22MnB5 and 30MnB5. However, the micro-alloyed steel of 34MnB5 type did not practically exhibit a correlation between PAGS and $\Delta R_{p0.2.}$
- A correlation between baking-induced decrease in Rm, i.e., softening of martensitic matrix and carbon content of the investigated PHS was observed: higher carbon content resulted in the larger decrease in R_m in general.
- Baking caused minor decrease (around 0.5 % on average) in uniform elongation (A_g), which is most likely connected to the precipitation of fine iron carbides and simultaneous relaxation of residual stresses during baking. The investigated 34MnB5 grade showed smaller changes in uniform elongation values.
- Distinct BH behavior of micro-alloyed 34MnB5 was observed in terms of $\Delta R_{p0.2}$ and ΔA_g. The behavior may be explained with the presence of (Ti, Nb)C carbides, which together with fine iron carbides and dislocation substructures control the mechanical behavior after the paint baking process.
- A typical paint baking procedure of automotive components clearly increased the post-uniform elongation of 34MnB5 with a carbon content of 0.35 %, whereas 22MnB5 and 30MnB5 with lower carbon contents of 0.23–0.29 % did not show significant changes in the post-uniform elongation or fracture behavior due to baking.
- It was shown that the combination of grain size (PAGS), carbon content (density of fine iron carbides), and distribution of coarse particles such as undissolved cementite determines the tensile behavior of bake hardened PHS.
- More research is still needed to understand the effect of individual chemical elements on the BH effect of PHS.

Acknowledgements: Mr. Tuomas Jokiaho is gratefully acknowledged for helping with the sample preparation routines of extraction replica techniques. The financial support (Grant no. 1235/13) of the Finnish Funding Agency for Technology and Innovation (Tekes) in the Breakthrough Steels and Applications Program of the Finnish Metals and Engineering Competence Cluster (FIMECC Ltd) is gratefully acknowledged. The financial support of Tampere University of Technology (TUT) in TUT's Graduate School is gratefully acknowledged.

References

Åkerström P, Modelling and Simulation of Hot Stamping, Doctoral Thesis, Luleå University of Technology, 2006.

Baker, L.J., Daniel, S.R., Parker, J.D., 2002. Metallurgy and processing of ultralow carbon bake hardening steels. Mater. Sci. Technol. 18, 355-68.

Bardelcik, A., Salisbury, C.P., Winkler, S., Wells, M.A., Worswick, M.J., 2010. Effect of cooling rate on the high strain rate properties of boron steel. Int. J. Impact Eng. 37, 694-702.

Choi, W.S., Lee, J., De Cooman, B.C., 2015. Internal-friction analysis of dislocation–interstitial carbon interactions in press-hardened 22MnB5 steel. Mater. Sci. Eng., A 639, 439-447.

Cottrell, A., Bilby, B., 1949. Dislocation Theory of Yielding and Strain Ageing of Iron. Proceedings of the Physical Society, Section A, 62 (1), 49-62.

Das, S., Timokhina, I., Singh, S.B., Pereloma, E., Mohanty, O.N., 2012. Effect of bainitic transformation on bake hardening in TRIP assisted steel. Mater. Sci. Eng., A 534, 485-494.

De, A.K., Vandeputte, S., Soenen, B., De Cooman, B.C. 2004. Effect of grain size on the static strain aging of a ULC-bake hardening steel. Zeitschrift für Metallkunde 95 (8), 713-717.

Fan, D., Kim, H., De Cooman, B., 2009. A Review of the Physical Metallurgy related to the Hot Press Forming of Advanced High Strength Steel. Steel Res. Int. 80, 241-248.

Galindo-Nava, E.I., Rivera-Díaz-del-Castillo, P.E.J., 2015. A model for the microstructure behaviour and strength evolution in lath martensite. Acta Mater. 98, 81-93.

Hagström, J., Ryde, L., 2008. Bake Hardening in Dual Phase and Martensitic High Strength Steels. Technical Report KIMAB-2008-101.

Hanai, S., Takemoto, N., Tokunaga, Y., Mizuyama, Y., 1984. Effect of Grain Size and Solid Solution on the Bake Hardenability of Low Carbon Strengthening Elements Aluminum-killed Steel. Trans. ISIJ 24, 17-23.

Hutchinson, B., Hagström, J., Karlsson, O., Lindell, D., Tornberg, M., Lindberg, F., Thuvander, M., 2011. Microstructures and hardness of as-quenched martensites (0.1–0.5%C). Acta Mater. 59, 5845-5858.

Hutchinson, B., Lindell, D., Barnett, M., 2015. Yielding Behaviour of Martensite in Steel. ISIJ Int. 55, 1114-1122.

International Centre for Diffraction Data (ICDD), 2015. ICDD card, 04-006-2103, PDF-4+ 2015 database.

Järvinen, H., Isakov, M., Nyyssönen, T., Järvenpää, M., Peura, P., 2016. The effect of initial microstructure on the final properties of press hardened 22MnB5 steels. Mater. Sci. Eng., A 676, 109-120.

Kantereit, H., 2011. Bake Hardening Behavior of Advanced High Strength Steels under Manufacturing Conditions. SAE Technical Paper 2011-01-1053.

Kennett, S.C., Krauss, G., Findley, K.O., 2015. Prior austenite grain size and tempering effects on the dislocation density of low-C Nb–Ti microalloyed lath martensite. Scr. Mater. 107, 123-126.

Kinoshita, M., Nishimoto, A. 1990. Effect of carbon content and grain size on bake-hardenability or aging property of extra-low carbon cold rolled steel sheet. CAMP-ISIJ 3, 1780-1785.

Krauss, G., 1999. Martensite in steel: strength and structure. Mater. Sci. Eng., A 273–275, 40-57.

Krauss, G., 1995. Heat Treated Martensitic Steels: Microstructural Systems for Advanced Manufacture. ISIJ Int. 35, 349-359.

Kuhlmann-Wilsdorf, D., 1989. Theory of plastic deformation: - properties of low energy dislocation structures. Mater. Sci. Eng., A 113, 1-41.

Labudde, T., Bleck, W., 2009. Formability characterisation of press hardened steels. In: Oldenburg, M., Steinhoff, K., Prakash, B. (Eds.), Proceedings of 2nd International Conference on Hot Sheet Metal Forming of High-Performance Steel, Luleå, Sweden, 127-135.

Larour, P., Pauli, H., Kurz, T., Hebesberger, T., 2010. Influence of post uniform tensile and bending properties on the crash behaviour of AHSS and press-hardening steel grades. Proceedings of International Conference IDDRG, Graz, Austria.

Leslie, W.C., Sober, R., 1967. Yielding and plastic flow in polycrystalline interstitial-free Fe 0.15 percent Ti Alloy. ASM Trans. Quart. 60, 99-111.

Matsuda, H., Mizuno, R., Funakawa, Y., Seto, K., Matsuoka, S., Tanaka, Y., 2013. Effects of auto-tempering behaviour of martensite on mechanical properties of ultra high strength steel sheets. J. Alloys Compd. 577, 661-667.

Miller, M.K., Beaven, P.A., Brenner, S.S., Smith, G.D.W., 1983. An atom probe study of the aging of iron- nickel- carbon martensite. Metall. Trans. A 14, 1021-1024.

Morito, S., Yoshida, H., Maki, T., Huang, X., 2006. Effect of block size on the strength of lath martensite in low carbon steels. Mater. Sci. Eng., A 438–440, 237-240.

Nishibata, T., Kojima, N., 2013. Effect of quenching rate on hardness and microstructure of hot-stamped steel. J. Alloys Compd. 577, 549-554.

Nyyssönen, T., Isakov, M., Peura, P., Kuokkala, V.-T., 2016. Iterative Determination of the Orientation Relationship between Austenite and Martensite from a Large Amount of Grain Pair Misorientations. Metall. Mater. Trans. A 47, 2587-2590.

Otani, S., Kozuka, M., Murakami, T., Naito, J., Pichler, A., Kurz, T., 2015. Metallurgical Controlling Factors for the Ductility of Hot Stamped Parts. In: Oldenburg, M., Steinhoff, K., Prakash, B. (Eds.), Proceedings of 5th International Conference on Hot Sheet Metal Forming of High Performance Steel, Toronto, Canada, 411-416.

Pereloma, E., Bata, V., Gazder, A.A., 2012. The effect of chromium addition on the strain ageing and recrystallisation behaviour of low carbon steel. In: Furuhara, T., Numakura, H., Ushioda, K. (Eds.), 3rd International Symposium on Steel Science (ISSS 2012), Kyoto, Japan, 41-50.

Saeglitz, M., Krauss, G., 1997. Deformation, fracture, and mechanical properties of low-temperature-tempered martensite in SAE 43xx steels. Metall. Mater. Trans. A 28, 377-387.

Saunders, N., Guo, U.K.Z., Li, X., Miodownik, A.P., Schille, J.-P., 2003. Using JMatPro to model materials properties and behavior. JOM. 55 (12), 60-65.

Sherman, A.M., Eldis, G.T., Cohen, M., 1983. The aging and tempering of iron-nickel-carbon martensites. Metall. Trans. A 14, 995-1005.

Snoek, J.L., 1941. Effect of small quantities of carbon and nitrogen on the elastic and plastic properties of iron. Physica 8, 711-733.

Sulistiyo, D.H., Cho, L., Seo, E.J., De Cooman, B.C., 2016. Internal friction analysis of lath martensite in press hardened steel. Mater. Sci. Technol. 33 (7), 1-14.

Timoknina, I., Hodgson, P., Ringer, S., Zheng, R., Pereloma, E., 2008. Understanding Bake-Hardening in Modern High Strength Steels for the Automotive Industry Using Advanced Analytical Techniques. In: Proceedings of the International Conference on New Developments on Metallurgy and Applications of High Strength Steels, Buenos Aires, Argentina.

Wilde, J., Cerezo, A., Smith, G.D.W., 2000. Three-dimensional atomic-scale mapping of a cottrell atmosphere around a dislocation in iron. Scr. Mater. 43, 39-48.

Wilson, D.V., Russell, B., 1960a. The contribution of atmosphere locking to the strain-ageing of low carbon steels. Acta Metall. 8, 36-45.

Wilson, D.V., Russell, B., 1960b. The contribution of precipitation to strain ageing in low carbon steels. Acta Metall. 8, 468-479.

Wilson, D.V., Russell, B., Eshelby, J.D., 1959. Stress induced ordering and strain-ageing in low carbon steels. Acta Metall. 7, 628-631.

Wu, H., Ju, B., Tang, D., Hu, R., Guo, A., Kang, Q., Wang, D., 2015. Effect of Nb addition on the microstructure and mechanical properties of an 1800 MPa ultrahigh strength steel. Mater. Sci. Eng., A 622, 61-66.

Zhang, C., Wang, Q., Ren, J., Li, R., Wang, M., Zhang, F., Sun, K., 2012. Effect of martensitic morphology on mechanical properties of an as-quenched and tempered 25CrMo48V steel. Mater. Sci. Eng., A 534, 339-346.